A Novel High-Order Symplectic Compact FDTD Schemes for Optical Waveguide Simulation

Xiaojing Kuang ⓘ, Zhixiang Huang ⓘ, *Senior Member, IEEE*, Ming Fang ⓘ,
Qi Qi ⓘ, Mingshen Chen ⓘ, and Xianliang Wu

Abstract—As a 2-D full-wave numerical algorithm in the time domain, the compact Finite Difference Time Domain (FDTD) is an efficient algorithm for eigenvalue analysis of optical waveguide system. However, the numerical dispersion accuracy and stability of fast algorithm need to be improved while simulating at high frequency. A novel high-order symplectic compact FDTD scheme is developed and validated for optical waveguide modal analysis. The stability condition and the numerical dispersion of schemes with fourth-order accuracy in temporal and spatial using the symplectic integrator and compact scheme are analyzed. By comparisons with other time-domain schemes, their stable and accurate performance is qualitatively verified. The proposed high-order SC-FDTD method can be used for efficiently simulating electrically large and longitudinally invariant optical devices since the reduction of simulation dimensionality and the novel high-order symplectic algorithm can greatly reduce the memory cost and the numerical dispersive errors.

Index Terms—Finite-difference time-domain, symplectic integrator, compact-scheme, optical waveguide.

I. INTRODUCTION

RESEARCH on the analytical method of eigenvalue problem is an important topic in optical devices. As a full-wave numerical scheme in the time domain, the finite-difference time-domain (FDTD) method has been extensively used for modeling computational electromagnetic in optical waveguide system [1], [2]. The FDTD method has the advantages of physical intuitive, easy to implement, and efficient. It can capture a broad frequency range with just a single simulation, and can investigate nonlinear electrodynamics in a natural way [3]–[5]. Thus, FDTD method has been applied to optical devices analyses at the nanometer scale, such as spaser, nanoscale waveguide, nanolasers, and solar cells [6]–[10]. However, this algorithm needs to scale down the time step to mitigate the numerical dispersion errors while simulating at high frequency. Especially in dealing with the field pattern and transmission characteristics of different modes in the optical waveguide simulation [11]–[13]. It takes plenty of computing resources and time since they are several tens to several thousand times larger than the wavelength in them. Therefore, it is an urgent problem to study the efficient time-domain algorithm for solving the eigenvalue problem of optical guided wave structures.

In view of the particularity of solving the eigenvalue problem of an optical guided wave system. The refractive index profile is invariant along the propagation direction, thus, the electromagnetic wave has the same optical field distribution on any cross-section. In this case, the compact-FDTD (C-FDTD) scheme has been proposed by Xiao *et al.*, in which all the field information about the three-dimensional structure can be extracted from its two-dimensional cross-section [14]–[20]. Though the computing resources and times has reduced by the fast algorithm, the accurate performance cannot be guaranteed. Then, the high-order spatial differencing scheme has been researched by Hadi and Mahmoud [21]. Although the spatial accuracy can be slightly improved by the high-order spatial schemes, it is also subjected to CFL stability condition. In order to further develop a nondissipative scheme for mitigating the error of the C-FDTD scheme. Other high-order temporal differencing schemes are also attracting attention [22]–[24].

Recently, based on higher-order symplectic integrator temporal algorithm for energy conservation and compact spatial algorithm for dimensional reduction, a novel high-order symplectic compact FDTD (SC-FDTD) scheme is proposed. The novel scheme is different from the previously proposed schemes, which follow the improvement on the above mentions. Combined symplectic integrator temporal scheme for energy conservation with the compact spatial scheme for dimensional reduction, the scheme not only guarantees simulation precision but also ensures the high efficiency of the simulation. Firstly, the scheme establishes a new high-order spatio-temporal matching evolution matrix in which the fast evolution matrix of spatial dimension reduction and the Hamiltonian matrix of temporal symplectic integral for Maxwell's equations, which has energy-conserving characteristics for long-range propagation [25], [26]. Secondly, the appropriate propagation constant has selected into the matrix and vector wave function

Xiaojing Kuang, Qi Qi, and Mingshen Chen are with the Anhui Province Key Laboratory of Simulation and Design for Electronic Information System, Hefei Normal University, Hefei 230061, China (e-mail: ziranisbest@163.com; microwaveqq@126.com; chenms@ustc.edu.cn).

Zhixiang Huang, Ming Fang, and Xianliang Wu are with the Key Laboratory of Intelligent Computing & Signal Processing, Ministry of Education, Anhui University, Hefei 230601, China (e-mail: zxhuang@ahu.edu.cn; mingfang@ahu.edu.cn; xlwu@ahu.edu.cn).

expansion. Thirdly, the novel scheme optimization of the various key technologies which contain numerical stability, numerical dispersion, and absorption boundary conditions are researched. Especially, different from the multi-image technique used in the time-domain multi-resolution algorithm is adopted on the metal truncation boundary, when solving the eigenvalue problem of metal resonator [28]. The split-field can be used to construct the higher-order PML absorption boundary conditions, when dealing with eigenvalue problems of complex dielectric resonators and photonic crystals. Comparisons with other time-domain algorithms, the advantages of the novel scheme is verified by the analysis of numerical stability and accuracy in long time simulation. One can find that the global dispersion error can be effectively improved by the novel scheme at the same accuracy of time due to the nondissipative characteristic of symplectic integrator temporal scheme. Furthermore, the novel scheme can be made nearly independent of the maximum limitation of the Courant Friedrich Levy law, which largely enhances the computational efficiency without improving precision by using excessive fine subdivision. This paper presents the details of the scheme and describes its basic properties, and is demonstrated by numerical experiment on long-term simulation of dielectric optical waveguides with complex cross-sections and photonic crystal fiber.

II. METHOD AND THEORY SCHEMES

A. Schemes

In the passive, uniform and lossless media, using the theoretical background of the symplectic properties [27], the Hamilton function of Maxwell's curl equations is defined as follows:

$$\Xi(\mathbf{H}, \mathbf{E}) = \frac{1}{2}\left(\frac{1}{\varepsilon}\mathbf{H}\cdot\nabla\times\mathbf{H} + \frac{1}{\mu}\mathbf{E}\cdot\nabla\times\mathbf{E}\right). \quad (1)$$

According to the variational principle, the above equation is rewritten into the matrix form:

$$\frac{\partial}{\partial t}\begin{pmatrix}\mathbf{H}\\\hat{\mathbf{E}}\end{pmatrix} = L\begin{pmatrix}\mathbf{H}\\\hat{\mathbf{E}}\end{pmatrix}, \quad L = U + V \quad (2)$$

where

$$U = \begin{pmatrix}\{0\}_{3\times3} & -\frac{1}{\sqrt{\mu\varepsilon}}\Re\\\{0\}_{3\times3} & \{0\}_{3\times3}\end{pmatrix},$$

$$V = \begin{pmatrix}\{0\}_{3\times3} & \{0\}_{3\times3}\\\frac{1}{\sqrt{\mu\varepsilon}}\Re & \{0\}_{3\times3}\end{pmatrix},$$

$$\Re = \begin{pmatrix}0 & -\frac{\partial}{\partial z} & \frac{\partial}{\partial y}\\\frac{\partial}{\partial z} & 0 & -\frac{\partial}{\partial x}\\-\frac{\partial}{\partial y} & \frac{\partial}{\partial x} & 0\end{pmatrix}, \quad (3)$$

where **E** and **H** are the electric and magnetic field vectors, ε and μ are the permittivity and permeability of the space. In order to get the compact spatial scheme, replacing the z-derivative (assumed the propagation direction along the z-axis) with the -$j\beta$ term, the three-dimensional curl operator $\Re$ can be rewritten as:

$$\Re = \begin{pmatrix}0 & j\beta & \frac{\partial}{\partial y}\\-j\beta & 0 & -\frac{\partial}{\partial x}\\-\frac{\partial}{\partial y} & \frac{\partial}{\partial x} & 0\end{pmatrix}. \quad (4)$$

The time evolution of (2) from time $t = 0$ to $t = \Delta_t$ are obtained:

$$\begin{pmatrix}\mathbf{H}\\\hat{\mathbf{E}}\end{pmatrix}(\Delta_t) = \exp(\Delta_t L)\begin{pmatrix}\mathbf{H}\\\hat{\mathbf{E}}\end{pmatrix}(0). \quad (5)$$

Here, $\hat{\mathbf{E}}$ is defined by the normalized electric field. Δ_t is the time step temporal. The evolution matrix $\exp(\Delta_t L)$ can be approximated by the mth-stage pth-order symplectic integrator scheme:

$$\exp(\Delta_t(U+V)) = \prod_{l=1}^{m}\exp(d_l\Delta_t V)\exp(c_l\Delta_t U) + O\left(\Delta_t^{p+1}\right), \quad (6)$$

where c_l and d_l are the constant coefficients of pth-order temporal symplectic operators. The $\exp(c_l\Delta_t U)$ and $\exp(c_l\Delta_t U)$ are basic symplectic transformations at each time step, which completes the display iteration between electric field and magnetic field components f. Meanwhile, the qth-order staggered central difference scheme with the 2-D Yee lattice is used to approximate the first-order spatial derivatives. The operator ς(x-, y-component) are derived as follows:

$$\varsigma_x \approx \sum_{r=1}^{q/2} W_r\frac{f(i+r+1/2,j)-f(i-r+1/2,j)}{h}, \quad (7a)$$

$$\varsigma_y \approx \sum_{r=1}^{q/2} W_r\frac{f(i,j+r+1/2)-f(i,j-r+1/2)}{h}, \quad (7b)$$

where h is the mesh size and W_r is the qth-order spatial difference coefficient. Then, the appropriate propagation constant is selected into the matrix and vector wave function expansion. The novel high-order symplectic compact FDTD (SC-FDTD(p,q)) formulation can be deduced as (8) shown at the bottom of this page:

Therefore, a new high-order spatio-temporal matching evolution matrix in which the fast evolution matrix of spatial dimension reduction and the Hamiltonian matrix of temporal symplectic integral are combined. Here, $p = 4$ and $q = 4$ are used, and the explicit fourth-order accurate difference coefficients are $W_1 = 9/8$ and $W_2 = -1/24$. The SC-FDTD (44) updated

$$\begin{pmatrix}\boldsymbol{H}\\\hat{\boldsymbol{E}}\end{pmatrix}\Bigg|_{t=\Delta_t} = \prod_{l=1}^{m}\begin{pmatrix}\{I\}_{3\times3} & 0\\\frac{1}{\varepsilon}\begin{pmatrix}0 & j\beta & \varsigma_y\\-j\beta & 0 & -\varsigma_x\\-\varsigma_y & \varsigma_x & 0\end{pmatrix}d_l\Delta_t & \{I\}_{3\times3}\end{pmatrix}\begin{pmatrix}\{I\}_{3\times3} & -\frac{1}{\mu}\begin{pmatrix}0 & j\beta & \varsigma_y\\-j\beta & 0 & -\varsigma_x\\-\varsigma_y & \varsigma_x & 0\end{pmatrix}c_l\Delta_t\\0 & \{I\}_{3\times3}\end{pmatrix}\begin{pmatrix}\boldsymbol{H}\\\hat{\boldsymbol{E}}\end{pmatrix}\Bigg|_{t=0}. \quad (8)$$

equations can be derived accordingly. For the sake of brevity, only the *x* component of **E** and **H** fields are given as follows:

$$\hat{E}_x^{n+l/m}(i+\tfrac{1}{2},j) = \hat{E}_x^{n+(l-1)/m}(i+\tfrac{1}{2},j)$$
$$+\tfrac{1}{\varepsilon_r(i+\tfrac{1}{2},j)}$$
$$\times\left\{\alpha_{y1}\times\left[H_z^{n+l/m}(i+\tfrac{1}{2},j+\tfrac{1}{2}) - H_z^{n+l/m}(i+\tfrac{1}{2},j-\tfrac{1}{2})\right]\right.$$
$$+\alpha_{y2}\times\left[H_z^{n+l/m}(i+\tfrac{1}{2},j+\tfrac{3}{2}) - H_z^{n+l/m}(i+\tfrac{1}{2},j-\tfrac{3}{2})\right],$$
$$\left.+\gamma_z\times\left[H_y^{n+l/m}(i+\tfrac{1}{2},j)\right]\right\}$$

$$(9\mathrm{a})$$

$$H_x^{n+l/m}(i,j+\tfrac{1}{2}) = H_x^{n+(l-1)/m}(i,j+\tfrac{1}{2})$$
$$+\tfrac{1}{\mu_r(i,j+\tfrac{1}{2})}\times\left\{\gamma_z\times\left[\hat{E}_y^{n+(l-1)/m}(i,j+\tfrac{1}{2})\right]\right.$$
$$-\gamma_{y1}\times\left[\hat{E}_z^{n+(l-1)/m}(i,j+1) - \hat{E}_z^{n+(l-1)/m}(i,j)\right],$$
$$\left.-\gamma_{y2}\times\left[\hat{E}_z^{n+(l-1)/m}(i,j+2) - \hat{E}_z^{n+(l-1)/m}(i,j-1)\right]\right\}$$

$$(9\mathrm{b})$$

where

$$\alpha_{\delta1} = \frac{9}{8}d_l\times CFL_\delta,\ \alpha_{\delta2} = \frac{-1}{24}d_l\times CFL_\delta,\ \gamma_{\delta1}$$

$$= \frac{9}{8}c_l\times CFL_\delta,$$

$$\gamma_{\delta2} = \frac{-1}{24}c_l\times CFL_\delta,\ \gamma_z = \beta\times CFL_z\times\Delta_z, \qquad (10)$$

in which

$$CFL_\delta = \frac{1}{\sqrt{\mu_0\varepsilon_0}}\frac{\Delta_t}{\Delta_\delta},\ \delta = x,y, \qquad (11)$$

where ε_r denotes the relative permittivity at point $(i+1/2, j)$, and $\Delta_x = \Delta_y = \Delta_z = h$ is the mesh size.

B. Stability Conditions Criteria

Reviewing background knowledge of the stability condition of the symplectic algorithm [27], it may be helpful to understand the numerical stability of SC-FDTD algorithm. Firstly, the updated field vectors **F** from time $t = n$ to $t = n+1$ meeting the following conditions:

$$\mathbf{F}^{n+1} = \mathbf{S}\cdot\mathbf{F}^n, \qquad (12)$$

where, **S** is the stability matrix of the symplectic algorithm. If the algorithm is stable, the sufficient and necessary condition is that all eigenvalues modulus of the matrix **S** is less than or equal to 1.

According to the (8) of SC-FDTD(p, q) algorithm, the stability matrix **S** can be obtained as follows (13) shown at the bottom of this page:

TABLE I
THE MAXIMUM VALUES OF CFL NUMBER

Methods	CFL_{max}
FDTD(2,2)	0.577
S-FDTD(4,4)	0.743
C-FDTD(2,2)	0.557
SC-FDTD(4,4)	0.916

The eigenvalue equation of matrix **S** is expressed as:

$$\lambda^2 - tr(\mathbf{S})\lambda + 1 = 0. \qquad (14)$$

By multiplying (13) in turn, we can get the trace of matrix **S**:

$$tr(\mathbf{S}) = 2 + \sum_{l=1}^{m} g_l\left\{v_0^2\Delta_t^2\left(\varsigma_x^2+\varsigma_y^2+\beta^2\right)\right\}^l, \qquad (15)$$

in which

$$v_0 = \frac{1}{\sqrt{\mu_0\varepsilon_0}}, \qquad (16\mathrm{a})$$

$$g_l = \sum_{1\leq i_1\leq j_1<i_2\leq j_2<\cdots<i_l\leq j_l\leq m} c_{i_1}d_{j_1}c_{i_2}d_{j_2}\cdots c_{i_l}d_{j_l}$$
$$+ \sum_{1\leq i_1<j_1\leq i_2<j_2\leq\cdots\leq i_l<j_l\leq m} d_{i_1}c_{j_1}d_{i_2}c_{j_2}\cdots d_{i_l}c_{j_l}. \qquad (16\mathrm{b})$$

In order to meet the requirement of stability condition, the eigenvalues modulus of the (14) is equal to 1, as long as, that is satisfying $|tr(\mathbf{S})| \leq 2$. According to (15), the CFL number of the SC-FDTD(44) can be obtained:

$$CFL \leq \frac{3}{2}\cdot\frac{1}{Q}, \qquad (17)$$

in which

$$Q = \left[\frac{9}{8}\sin\left(\frac{k_x\Delta_x}{2}\right) - \frac{1}{24}\sin\left(\frac{3k_x\Delta_x}{2}\right)\right]^2$$
$$+ \left[\frac{9}{8}\sin\left(\frac{k_y\Delta_y}{2}\right) - \frac{1}{24}\sin\left(\frac{3k_y\Delta_y}{2}\right)\right]^2$$
$$+ \left[\frac{9}{8}\left(\frac{\beta\Delta_z}{2}\right)^2 - \frac{1}{24}\left(\frac{\beta\Delta_z}{2}\right)^2\right]^2. \qquad (18)$$

As β_0 is the unbounded wave number, $\beta = 0.99\beta_0$ is defined. Concerning the values of different algorithms, the SC-FDTD(44) algorithm has the largest CFL_{max} number as illustrated in Table I. The results show that the new algorithm is more stable than other algorithms.

$$\mathbf{S} = \prod_{l=1}^{m}\left(\begin{array}{cc} \{I\}_{3\times3} & 0 \\ \frac{1}{\varepsilon}\begin{pmatrix} 0 & j\beta & \varsigma_y \\ -j\beta & 0 & -\varsigma_x \\ -\varsigma_y & \varsigma_x & 0 \end{pmatrix}d_l\Delta_t & \{I\}_{3\times3} \end{array}\right)\left(\begin{array}{cc} \{I\}_{3\times3} & -\frac{1}{\mu}\begin{pmatrix} 0 & j\beta & \varsigma_y \\ -j\beta & 0 & -\varsigma_x \\ -\varsigma_y & \varsigma_x & 0 \end{pmatrix}c_l\Delta_t \\ 0 & \{I\}_{3\times3} \end{array}\right). \qquad (13)$$
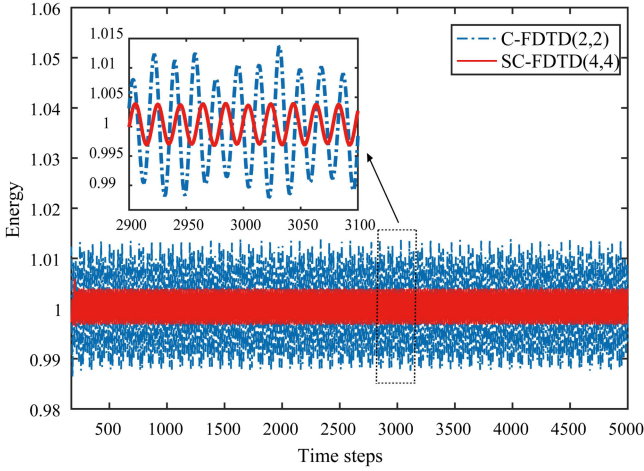
Fig. 1. Normalized energy at each time step.

C. Numerical Dispersion Analysis

According to (14), the new algorithm is dissipative when the stability condition meets $|\lambda_{1,2}| = 1$. So, the phase Angle of the eigenvalue can be calculated by the arccosine, and the dispersion-free equation can be expressed as [27]:

$$\cos(\omega \Delta t) = tr(\mathbf{S})/2. \tag{19}$$

Substitute into the expression of (16), the dispersion relation equation (15) can be rewritten as:

$$\sin^2\left(\frac{\omega \Delta t}{2}\right) + \frac{1}{4}\sum_{l=1}^{m} g_l\{(-4)\cdot v_0^2 \cdot \Delta^2_t \cdot Q\}^l = 0, \tag{20}$$

in which, k_x and k_y are, respectively, numerically rendered transverse wave number for x-, y-direction.

By the dispersion (20), the numerical global phase error Φ is depended on several factors, such as the normalized propagation constant ($\kappa = \beta / \beta_0$), the courant number ($\nu = \Delta_{tmax} / \Delta_t$) and the resolution factor ($R = \lambda_T / h$). For the influence of the above factors on the global phase error Φ, we have made a detailed study of the comprehensive comparisons of global phase errors between the proposed algorithm SC-FDTD(4, 4) and other algorithms in reference [28]. One can find that the global phase error of SC-FDTD(4, 4) algorithm is far below that of the other methods at the same accuracy condition.

In order to verified that the nondissipative characteristic of symplectic integrator temporal derivatives in SC-FDTD(4, 4) algorithm. A comparative study of the normalized energy at each time step is shown in Fig. 1. Note that the amplitude of the energy oscillation of SC-FDTD (4, 4) algorithm is closer around the exact value than that of C-FDTD(2, 2) algorithm. This conclusion suggests that the SC-FDTD (4, 4) algorithm can achieve energy-conserving.

As the normalized propagation constant approaches unity, rigorous dispersion analysis will follow which the global phase error deterioration and the time step is kept at the maximum limit allowed by the dispersion relation (20) for each κ value. Further analysis of the normalized propagation constant κ and

the resolution factor R have critical role to play in minimizing numerical global phase errors Φ. A comprehensive comparisons of global phase error between SC-FDTD(4, 4) and C-S$_{24}$[5], [7] at the same time step Δ_{tmax} for different R and κ is shown in Table II. It be clearly seen that the error of SC-FDTD(4, 4) algorithm is far below that of the C-S$_{24}$ algorithm at any value κ and R. Meanwhile, the excessively high resolution factors R are needed near the limiting value of κ approaches unity of the C-S$_{24}$ algorithm. Or more courant number ν_{opt} are required to improve the error of the C-S$_{24}$ algorithm. However, the SC-FDTD (4, 4) algorithm can be made nearly independent of the maximum limitation of the Courant Friedrich Levy law, which largely enhances the computational efficiency without improving precision by using excessive fine subdivision.

D. PML Absorption Boundary Condition

Similar to the treatment for Maxwell equations in S-FDTD algorithm[27], PML for the SC-FDTD updated equations in (9a) and (9b) are derived by incorporating high-order exponential difference techniques in dealing with complex dielectric resonators, photonic crystals and open or half-open eigenvalue problems. Considering the different forms of Maxwell equations in the time domain under the split field in three dimensions, our following derivations will be made to E_x and H_x component only, as other field components can be treated in a similar manner.

$$
\begin{cases}
\hat{E}_{xy}^{n+l/m}(i+\tfrac{1}{2},j) = \exp(-\xi_y) \times \hat{E}_{xy}^{n+(l-1)/m}(i+\tfrac{1}{2},j) \\
+\frac{1-\exp(-\xi_y)}{\xi_y} \\
\times \Big\{\alpha_{y1}\times\big[H_z^{n+l/m}(i+\tfrac{1}{2},j+\tfrac{1}{2})-H_z^{n+l/m}(i+\tfrac{1}{2},j-\tfrac{1}{2})\big] \\
+\alpha_{y2}\times\big[H_z^{n+l/m}(i+\tfrac{1}{2},j+\tfrac{3}{2})-H_z^{n+l/m}(i+\tfrac{1}{2},j-\tfrac{3}{2})\big]\Big\}, \\
\hat{E}_{xz}^{n+l/m}(i+\tfrac{1}{2},j) = \exp(-\xi_z) \times \hat{E}_{xz}^{n+(l-1)/m}(i+\tfrac{1}{2},j) \\
+\frac{1-\exp(-\xi_z)}{\xi_z} \\
\times \Big\{\gamma_z \times \big[H_y^{n+l/m}(i+\tfrac{1}{2},j)\big]\Big\}
\end{cases}
\tag{21a}
$$

in which

$$\xi_\delta = \frac{d_l \Delta_t \sigma_\delta(i+\tfrac{1}{2},j)}{\varepsilon_0(i+\tfrac{1}{2},j)}, \delta = y,z, \tag{21b}$$

$$
\begin{cases}
H_{xy}^{n+l/m}(i,j+\tfrac{1}{2}) = \exp(-\xi_y) \\
\times H_{xy}^{n+(l-1)/m}(i,j+\tfrac{1}{2}) + \frac{1-\exp(-\xi_y)}{\xi_y} \\
\times \Big\{-\gamma_{y1}\times\big[\hat{E}_z^{n+(l-1)/m}(i,j+1)-\hat{E}_z^{n+(l-1)/m}(i,j)\big] \\
-\gamma_{y2}\times\big[\hat{E}_z^{n+(l-1)/m}(i,j+2)-\hat{E}_z^{n+(l-1)/m}(i,j-1)\big]\Big\}, \\
H_{xz}^{n+l/m}(i,j+\tfrac{1}{2}) = \exp(-\xi_z) \\
\times H_{xz}^{n+(l-1)/m}(i,j+\tfrac{1}{2}) + \frac{1-\exp(-\xi_z)}{\xi_z} \\
\times \Big\{\gamma_z \times \big[E_y^{n+l/m}(i+\tfrac{1}{2},j)\big]\Big\}
\end{cases}
\tag{22a}
$$

in which

$$\xi_\delta = \frac{c_l \Delta_t \sigma_\delta(i,j+\tfrac{1}{2})}{\varepsilon_0(i,j+\tfrac{1}{2})}, \delta = y,z. \tag{22b}$$

TABLE II
A COMPARATIVE SUMMARY OF THE FORMATION IN SIMULATIONS USING DIFFERENT METHODS FOR DIFFERENT R AND κ

| R, κ	Algorithm	ν_{opt}	ν	$\Delta_{t\,max}$	Δ_t	Φ at ν_{opt}
$R=10$	SC-FDTD(4,4)	4	-	3.1119e-10	7.7797e-11	1.0e-5
and	C-S$_{24}$	6	-	2.9332e-10	4.8886e-11	1.2e-2
$\kappa=0.95$		-	4	2.9332e-10	7.7797e-11	1.8e-1
$R=10$	SC-FDTD(4,4)	4	-	3.0619e-10	7.6525e-11	3.4e-7
and	C-S$_{24}$	60	-	2.8411e-10	4.7351e-12	4.8e-6
$\kappa=0.99$		-	4	2.8411e-10	7.6525e-11	1.5e-0
$R=20$	SC-FDTD(4,4)	4	-	1.8328e-10	4.5820e-11	2.0e-9
and	C-S$_{24}$	190	-	2.2068e-10	1.1614e-12	1.9e-8
$\kappa=0.99$		-	5	2.2068e-10	4.5820e-11	2.2e-1
$R=30$	SC-FDTD(4,4)	4	-	1.2741e-10	3.1852e-11	2.9e-10
and	C-S$_{24}$	325	-	1.7122e-10	4.2003e-14	7.9e-10
$\kappa=0.99$		-	5.4	1.7122e-10	3.1852e-11	8.2e-2
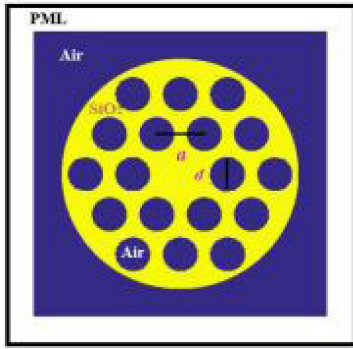
Fig. 2. The modal of the photonic crystal fiber structure in this simulation, the diameter of the air hole column ($d = 1\ \mu m$), the lattice size of the air hole column $a = 5\ \mu m$, and the air hole column is coated with silica material.

III. NUMERICAL RESULTS

The dispersive characteristic is an important parameter of a longitudinally invariant optical waveguide structure in engineering practice [29]–[33]. To validate our algorithm, the dispersive characteristics of photonic crystal fiber is simulated by SC-FDTD(44) algorithm and compared with the results of FEM. The modal of the photonic crystal fiber is shown in Fig. 2. Firstly, the propagation constant and the excitation source are defined beforehand. Secondly, the Maxwell equations of the main and PML areas are discretized by using the high-order symplectic compact difference scheme. Thirdly, the six field components of the electromagnetic field are staggered and iterated in the grid until the steady-state is reached, and then the time-domain field value is output. Finally, the frequency value is obtained through the Fourier transform, and then modal analysis can be carried out. The same propagation constant corresponds to different propagation modes in the same physical size, of which the fundamental mode has the longest wavelength. On the contrary, the fundamental mode corresponds to different wavelengths under different propagation constants.
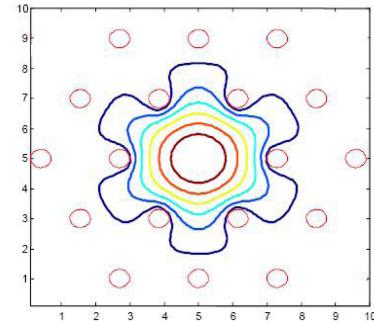
(a)
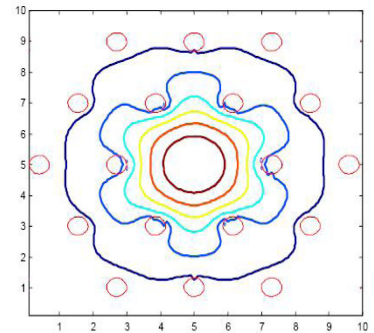
(b)

Fig. 3. Equipotential lines of the electric field component with continuous varying wavelengths. (a) $\lambda = 0.6\mu m$. (b) $\lambda = 1.5\mu m$.

Here, the propagation constants are selected to be 15e6 *rad/m* and 6e6 *rad/m*, respectively. Meanwhile, the corresponding fundamental mode wavelength is chosen as 0.6 μm and 1.5 μm, respectively. By continuous varying wavelength, equipotential lines of the electric field component are shown in Fig. 3.

It can be seen that the propagation of the light in the fiber is affected by the structure of the air hole column. When the value of *d/a* is larger than a critical value, the effective refractive index of the cladding region composed of the air hole column, and the medium is lower than the effective refractive index of
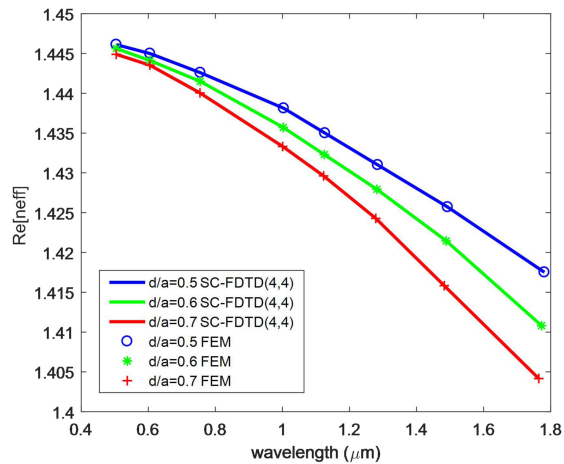
Fig. 4. The variation of effective refractive index with wavelength and propagation constant under different structures.

the medium core. Therefore, the light wave field is limited in the fiber core to achieve the total reflection phenomenon. whereas, the generation of total reflection is related to the effective refractive index. So, we consider that the variation of effective refractive index with wavelength and propagation constant under different structures are shown in Fig. 4. Here, the value of *d/a* are set to 0.5; 0.6; 0.7 when a is set to 5 μm. It can be seen that the SC-FDTD(44) algorithm is exactly consistent with the numerical results of the FEM. So, the correctness of the proposed algorithm can be verified. Furthermore, the simulation time and memory cost of the proposed algorithm are reduced to 1/10 and 1/3 of the FEM algorithm at the same accuracy condition.

IV. CONCLUSION

To study the efficient time-domain schemes for saving a lot of computational time and memory of photonic crystal fiber structures. a novel high-order symplectic compact FDTD scheme is proposed, which is attributed to the theory combination of the fast-spatial scheme and stable temporal scheme. The stability condition and the numerical dispersion of schemes with fourth-order accuracy in temporal and spatial using the symplectic integrator and compact scheme are derived. By comparisons with other time-domain schemes, their stable and accurate performance is qualitatively verified and is also demonstrated by numerical experiment on long-term simulation of dielectric optical waveguides with complex cross-sections and photonic crystal fiber.

REFERENCES

[1] D. M. Sullivan, "Electromagnetic simulation using the FDTD method," in the *Institute of Electrical and Electronics Engineers*, New York, NY, USA: IEEE Press, 2000, pp. 79–89.

[2] S. C. H. Taflove, "Computational electromagnetics: The finite-difference time-domain method," *Elect. Eng. Handbook*, no. 5, pp. 629–670, 2005.

[3] M. Fang, Z. X. Huang, T. Koschny, and C. M. Soukoulis, "Electrodynamic modeling of quantum dot luminescence in plasmonic metamaterials," *ACS Photon.*, vol. 3, no. 4, pp. 558–563, 2016.

[4] M. Fang, Z. X. Huang, and W. Sha, "Full hydrodynamic model of nonlinear electromagnetic response in metallic metamaterials," *Prog. Electromagnetics Res.*, vol. 157, pp. 63–78, 2016.

[5] M. Fang, K. K. Niu, and Z. X. Huang, "Investigation of broadband terahertz generation from metasurface," *Opt. Exp.*, vol. 26, no. 11, pp. 14241–14250, 2018.

[6] A. S. M. Mohsin and M. B.Salim, "Probing the plasmon coupling, quantum yield and effects of tip geometry of gold nanoparticle using analytical models and FDTD simulation," *IEEE Photon. J.*, vol. 10, no. 3, Jun. 2018, Art. no. 4800610.

[7] H. Y. Li, X. G. Luo, L. S. Yan, K. H. Wen, Z. Guo, and J. Chen, "Polarization and transmission properties of metamaterial-based three-dimensional plasmonic structure," *IEEE Photon. J.*, vol. 3, no. 3, pp. 721–729, Jun. 2011.

[8] G. G. Zheng *et al.*, "Optical filter and sensor based on plasmonic-gap-waveguide coupled with T-shaped resonators," *Optik - Int. J. Light Electron Opt.*, vol. 126, no. 23, pp. 4056–4060, 2015.

[9] Z. X. Huang, L. L. Cheng, and X. L. Wu, "The study of optical and electrical properties of short-pitch plasmonic solar cells," *IEEE Photon. J.*, vol. 8, no. 4, Aug. 2016, Art. no. 4802109.

[10] Z. X. Huang, L. L. Cheng, B. Wu, and X. L. Wu, "The study of optical and electrical properties of solar cells with oblique incidence," *IEEE Photon. Technol. Lett.*, vol. 28, no. 19, pp. 2047–2049, Oct. 2016.

[11] K. R. Hiremath, R. Stoffer, and M. Hammer, "Coupled mode theory and FDTD simulations of the coupling between bent and straight optical waveguides," *Univ. Twente*, vol. 709, no. 1, pp. 366–377, 2017.

[12] H. Wang, W. Sha, Z. X. Huang, and X. L. Wu, "A novel eigenvalue algorithm for the complex band structure and eigenmodes of plasmonic crystals," *IEEE Photon. J.*, vol. 8, no. 2, Apr. 2016, Art. no. 4801510.

[13] Z. Chen and L. Yu, "Multiple fano resonances based on different waveguide modes in a symmetry breaking plasmonic system," *IEEE Photon. J.*, vol. 6, no. 6, Dec. 2014, Art. no. 4802208.

[14] S. Xiao, R. Vahldieck, and H. Jin, "Full-wave analysis of guided wave structures using a novel 2-D FDTD," *IEEE Microw. Guided Wave Lett.*, vol. 2, no. 5, pp. 165–167, May 1992.

[15] M. F. Hadi and S. F. Mahmoud, "Optimizing the compact-FDTD algorithm for electrically large waveguiding structures," *PIER*, vol. 75, pp. 253–269, 2007.

[16] J. A. Pereda, A. Vegas, and A. Prieto, "An improved compact 2D full-wave FDFD method for general guided wave structures," *Microw. Opt. Technol. Lett.*, vol. 38, no. 4, pp. 331–335, 2003.

[17] G. R. Zhou and X. Li, "Wave equation-based semivectorial compact 2-D-FDTD method for optical waveguide modal analysis," *J. Lightw. Technol.*, vol. 22, no. 2, pp. 677–683, 2004.

[18] M. B. Hossain and M. M. Rana, "An effective compact-FDTD wideband modeling of graphene conductivity," in *Proc. IEEE Int. Conf. Elect. Eng. Inf. Commun. Technol.*, Savar, Bangladesh, 2015, pp. 1–3.

[19] Y. C. Jiang, S. B. Liu, and H. F. Zhang, "Design of ultra-compact all optical half subtracter based on self-collimation in the two-dimensional photonic crystals," *Opt. Commun.*, vol. 356, pp. 325–329, 2015.

[20] A. Benouatas and M. L. Riabi, "Efficient MT-based compact FDTD algorithm for longitudinally-magnetized ferrite-loaded waveguides," *J. Electromagn. Anal. Appl.*, vol. 5, no. 1, pp. 16–22, 2013.

[21] M. F. Had and S. F. Mahmoud, "A high-order compact-FDTD algorithm for electrically large waveguide analysis," *IEEE Trans. Antennas Propag.*, vol. 56, no. 8, pp. 2589–2598, Aug. 2008.

[22] Z. Kang, X. Ma, and X. Zhuansun, "An efficient 2-D compact precise integration time-domain method for longitudinally invariant waveguiding structures," *IEEE Trans. Microw. Theory Techn.*, vol. 61, no. 7, pp. 2535–2544, Jul. 2013.

[23] Z. Kang, X. Ma, and Q. Liu, "A high-order 2-D CPITD method for electrically large waveguide analysis," *IEEE Microw. Wireless Compon. Lett.*, vol. 26, no. 2, pp. 83–85, Feb. 2016.

[24] W. Sha, Z. Huang, M. Chen, and X. Wu, "Survey on symplectic finite-difference time-domain schemes for Maxwell's equations," *IEEE Trans. Antennas Propag.*, vol. 56, no. 2, pp. 493–500, Feb. 2008.

[25] H. Wang, B. Wu, Z. X. Huang, and X. L. Wu, "A symplectic FDTD algorithm for the simulations of lossy dispersive materials," *Comput. Phys. Commun.*, vol. 185, pp. 862–872, 2014.

[26] J. Shen, W. Sha, Z. X. Huang, M. S. Chen, and X. L. Wu, "High-order symplectic FDTD scheme for solving time-dependent schrödinger equation," *Comput. Phys. Commun.*, vol. 184, no. 3, pp. 480–492, 2013.

[27] W. Sha, Z. X. Huang, X. L. Wu, and M. S. Chen, "Application of the symplectic finite-difference time-domain scheme to electromagnetic simulation," *J. Comput. Phy*,vol. 2, no. 25, pp. 33–50, 2007.

[28] X. J. Kuang, Z. X. Huang, M. S. Chen, and X. L. Wu, "High-Order symplectic compact finite-different time-domain algorithm for guide-wave structures," *IEEE Microw. Wireless Compon. Lett.*, vol. 29, no. 2, pp. 80–82, Feb. 2019.

[29] J. D. Joannopoulos, S. G. Johnson, J. N. Winn, and R. D. Meada, *Photonic Crystals: Molding the Flow of Light*, Princeton, NJ, USA: Princeton Univ. Press, 2008.

[30] J. Broeng, D. Mogilevstev, and S. E. Barkou, "Photonic crystal fibers; a new class of optical waveguides," *Opt. Fiber Technol.*, vol. 5, no. 3, pp. 305–330, 1999.

[31] T. P. Hansen, J. Broeng, and S. E. B. Libori, "Highly birefringent index-guiding photonic crystal fibers," *IEEE Photon. Technol. Lett.*, vol. 13, no. 6, pp. 588–590, Jun. 2001.

[32] K. Tajima, "Recent progress of photonic crystal fibers," *Acta Optica Sinica*, vol. 23, no. 1, pp. 1528–1539, 2003.

[33] L. Shuqin, W. Zhi, and R. Guobin, "An efficient algorithm for modeling photonic crystal fibers," *Opt. Fiber Technol.*, vol. 11, no. 1, pp. 34–45, 2005.